2018-12

Ongoing evolution of submarine canyon rockwalls; examples from the Whittard Canyon, Celtic Margin (NE Atlantic)

Carter, GDO

10.1016/j.pocean.2018.02.001
Progress in Oceanography
Elsevier

This version is the Submitted Manuscript: 19 Jan 2018.
For Accepted and Online Article: https://doi.org/10.1016/j.pocean.2018.02.001
Available Online: 2 Feb 2018

Ongoing evolution of submarine canyon rockwalls; examples from the Whittard Canyon, Celtic Margin (NE Atlantic)

Gareth D.O. Carter[a*], Veerle A.I. Huvenne[b], Jennifer A. Gales[c], Claudio Lo Iacono[b], Leigh Marsh[b,d], Audrey Ougier-Simonin[e], Katleen Robert[b], and Russell B. Wynn[b]

[a] *British Geological Survey, The Lyell Centre, Research Avenue South, Edinburgh, EH14 4AP, UK*

[b] *Marine Geoscience, National Oceanography Centre, European Way, Southampton, SO14 3ZH, UK*

[c] *University of Plymouth, School of Biological and Marine Sciences, Drake Circus, Plymouth, PL4 8AA, UK*

[d] *Ocean and Earth Science, University of Southampton, Waterfront Campus, Southampton, SO14 3ZH, UK*

[e] *British Geological Survey, Environmental Science Centre, Nicker Hill, Keyworth, Nottingham, NG12 5GG, UK*

** Corresponding author: gcarter@bgs.ac.uk, +44 131 6500 373.*

ABSTRACT

During the CODEMAP 2015 research expedition to the Whittard Canyon, Celtic Margin (NE Atlantic), a Remotely Operated Vehicle (ROV) gathered High Definition (HD) video footage of the canyon rockwalls at depths of approx. 412 to 4184 mbsl. This dataset was supplemented by predominantly carbonate rock samples collected during the dives, which were subsequently tested for key physical property characteristics in a geotechnical laboratory. The high-resolution video footage revealed small-scale rockwall slope processes that would not have been visible if shipboard geophysical equipment was solely relied upon during the survey. Of particular interest was the apparent spalling failure of mudstone and chalk rockwalls, with fresh superficial "flaking" scars and an absence of sessile fauna possibly suggesting relatively recent mass-wasting activity. Extensive talus slopes, often consisting of coarse gravel, cobble and occasionally boulder-sized clasts, were observed at the foot of slopes impacted by spalling failures; this debris was rarely colonised by biological

communities, which could be an indicator of frequent rockfall events. Bio-erosion was also noted on many of the walls prone to this form of rock slope failure (RSF). As in subaerial equivalents, internal fracture networks appear to control the prevalence of RSF and the geometries of blocks, often resulting in cubic and tabular blocks (0.2-1.0 m scale) of bedrock toppling or sliding out of the cliff face. Tensile strength parameters of carbonate rock samples were determined and these may affect the mass wasting processes observed within the canyon. It was found that carbonate samples which appeared to have a higher mud content, and reduced porosity, produced significantly higher tensile strength values. It is proposed that these stronger, "muddy" carbonate units form the overhanging ledges that often provide an ideal setting for sessile species, such as *Acesta excavata* clams, to colonise whereas the weaker "pure" carbonate units are more easily eroded and therefore form the undercutting, receding sections of the rockwall.

By combining the ROV observations, basic discontinuity assessments (estimation of fracture orientations) and laboratory testing results, an understanding of the geomechanical properties of the bedrock can be obtained and linked with past and ongoing rock slope processes within the Whittard Canyon. These conclusions will have a wider implication for ongoing geomechanical processes within submarine canyons on a global scale.

Keywords: submarine canyons, bedrock erosion, bioerosion, canyon rockwalls, Celtic Margin, NE Atlantic, Whittard Canyon, Remotely Operated Vehicle

1. INTRODUCTION

Submarine canyons comprise dynamic environments in which physical and biological processes are constantly altering the slope morphology. The continuous transportation of unconsolidated sediments downslope, and occasionally upslope, by local hydrodynamic

forces has been well-documented within submarine canyons (e.g. Cunningham *et al*., 2005; Puig *et al*., 2014). Large-scale mass wasting processes and sedimentological down-canyon events such as turbidity currents are known to transport huge volumes of sediment through canyon systems (e.g. Sultan *et al*., 2007; Lo Iacono *et al*., 2011; Stewart *et al*., 2014; Sumner *et al*., 2014; Talling, 2014).

However, there are only limited examples of studies that have investigated the effects of bedrock processes on the morphology of submarine canyons. Despite submarine canyons providing an obvious subaqueous setting where steep, often subvertical or overhanging, bedrock terraces and cliffs are exposed at the seabed, very little research has been devoted to the study of small-scale present-day bedrock erosional processes within these environments and the subsequent consequences for ongoing canyon slope evolution. One example is the study by Micallef *et al* (2012) which presented evidence of deep-seated mass wasting of bedrock slopes within submarine canyons along the active tectonic margin of the Cook Strait, New Zealand. While Micallef *et al* (2012) provided excellent detail on large-scale bedrock landslides, including areas and volumes associated with slope failure events, small-scale bedrock erosional processes and their implications for canyon slope evolution were not discussed.

Chaytor *et al* (2016) did present evidence of small-scale bedrock failures within the canyons of the U.S. Atlantic Continental Margin, and linked these processes with structural controls within the bedrock units. However, the geomechanical properties of the different lithological units were not investigated in detail, and the influence of engineering characteristics (e.g. strength or porosity) upon bedrock slope erosion were not expanded upon with quantitative data. McHugh *et al* (1993) provide a detailed study on the role of diagenesis in the exfoliation of carbonate rocks within submarine canyons of the U.S. Atlantic Continental Margin (offshore New Jersey). Visual observations of bedrock erosion,

associated with joint network propagation due to diagenetic transformation, were linked with data collected by thin-section, scanning electron microscope/energy dispersive x-ray (SEM/EDX) analyses. However, as with Chaytor *et al* (2016), geomechanical properties were not investigated using geotechnical testing methods.

Previous studies from similar geological settings (e.g. Paull *et al* (1990a) focusing on subvertical to vertical limestone cliffs of the Florida Escarpment) have highlighted evidence of ongoing rock slope collapse. This suggests that the present-day slope profile of many subaqueous bedrock terraces and cliffs may have been altered over time by modern erosional processes.

External factors can also contribute to the erosion of canyon slopes, with bioerosion linked to benthic faunal communities being one source. A study by Dillon and Zimmerman (1970) in two New England submarine canyons identified outcrops of sandstone, siltstone and semi-consolidated mud that were riddled with burrows measuring up to 50 cm in diameter, which were often occupied by crustaceans such as crabs. Bioerosion of this nature has been noted in other U.S. submarine canyon systems (e.g. Warme *et al*., 1978; Valentine *et al*., 1980).

Large-scale slope failures, such as those described by Micallef *et al* (2012), and downslope sediment transfer processes (e.g. turbidity currents), as detailed by Sumner *et al* (2014), are known to transfer sediments from upper canyon realms down towards the canyon thalweg. However, what has not been well-documented to-date is the influence that small-scale bedrock erosional processes can have upon canyon dynamics in relation to inducing alterations to the geomorphology. In addition, when discussing mass transfer processes and sedimentary budgets within submarine canyons (e.g. Puig *et al*., 2003), bedrock erosional processes have frequently been overlooked as a source of seafloor material within canyon systems.

Many questions remain unanswered in relation to these erosional mechanisms; what processes are contributing to bedrock erosion in submarine canyons? What role do the geomechanical properties of different lithologies play in promoting ongoing slope erosion? To what extent do benthic faunal communities influence the morphology of submarine slopes and cliffs, including acting as a catalyst for slope erosion within canyon environments as suggested by several authors (e.g. Rowe, 1974; Hecker, 1982)?

Here we provide detailed video evidence collected during multiple Remotely Operated Vehicle (ROV) dives, highlighting small-scale present-day processes acting upon bedrock slopes within the Whittard Canyon, Celtic Margin. Measurement of the physical properties of rock samples collected from the canyon walls provide quantitative data, which are used to investigate the impact of bedrock structures and lithology on slope stability. The implications of these results on slope morphology and benthic habitats are discussed in the context of the Whittard Canyon, and more widely in terms of subaqueous rockwalls on a global scale.

2. GEOLOGICAL SETTING

The Whittard Canyon is a large dendritic canyon system extending from the shelf edge (approximately 200 m below sea level (mbsl)) to the base of the continental slope at approximately 4500 mbsl. It forms one of the most westerly of a number of submarine canyon complexes located along the passive Celtic Margin (NE Atlantic), approximately 300 km SSW of the Republic of Ireland (Figure 1). The continental slope has an average gradient of 8° in the vicinity of the Whittard Canyon, although it varies greatly across the Celtic Margin due to multiple gully and canyon incisions (Amaro *et al*., 2016). Towards the Goban Spur Margin, which bounds the western extent of the Whittard Canyon complex, the continental slope becomes more laterally continuous with an absence of slope incisions.

FIGURE 1 – FULL PAGE (SEPARATE FILE, CAPTION AT END OF MANUSCRIPT)

Laterally, this abrupt change in slope morphology is heavily influenced by changes in the underlying geological structure along the margin. However, the boundary between continental and oceanic crust consistently controls the base of the slope throughout the region, at approximately 4500 mbsl (Evans, 1990). The canyon itself was incised through retrogressive mass wasting of the slope and headwall, instigated during the Pliocene – Pleistocene (Amaro *et al*., 2016). Although it has previously been noted that there is very little or no evidence of present-day incision of the main axial channel (e.g. Stewart *et al*., 2014; Amaro *et al*., 2016), the evidence presented in this paper will demonstrate that the major bedrock units that form canyon rockwalls are in no way inert and erosional processes are ongoing.

The Early Cretaceous rifting episode of the North Atlantic resulted in the fault-block topography upon which the Celtic Margin formed. These rotated fault-blocks are thought to have influenced the profile of the lower slope, however the present day bathymetry of the upper slope is the result of erosional processes (e.g. slumping and sediment density currents) acting against the continued advancement of the shelf edge by sediment deposition (Evans, 1990).

The post-rifting stratigraphy comprises Cretaceous chalk, Paleogene limestones and mudstones, and Neogene calcareous clays, calcilutites (Jones Formation) and calcarenites (Cockburn Formation), capped by Pliocene to Pleistocene sediments of the Little Sole Formation (Evans & Hughes, 1984; Evans, 1990; Stewart *et al*., 2014). No borehole logs were available for the area of the shelf that immediately surrounds the canyon; however, British Geological Survey (BGS) and Deep Sea Drilling Project (DSDP) cores provide a general overview of the stratigraphy for the wider continental shelf and slope (Figure 1

(inset)). The Cretaceous chalks logged in BGS borehole +49-009/42 (Figure 2a), located approximately 118 km NE (shelfward) of the canyon head, are described as being white to pale grey, soft to firm, granular and glauconitic in places, and fossiliferous. Sporadic flint nodules are also noted. Elsewhere, DSDP cores (Figure 2b) record carbonaceous and marly nannofossil chalks of Cretaceous age (Montadert *et al*., 1979). Paleogene soft clays, firm to hard (and glauconitic in parts) limestone and fine-grained carbonaceous sandstone are present in BGS borehole +49-009/42, overlain by Neogene clays that are calcareous, glauconitic, carbonaceous and fossiliferous in nature. The DSDP borehole logs reveal siliceous mudstones, silicified limestones, marly nannofossil chalks and nannofossil ooze of Paleogene age, overlain by Neogene nannofossil chalks and oozes, siliceous mudstones, capped by Pleistocene calcareous muds and nannofossil oozes (Montadert *et al*., 1979). While these borehole locations are not immediately adjacent to the Whittard Canyon, the formations logged in these cores present a stratigraphic framework for the wider Celtic Margin into which the canyon is incised.

The oceanographic conditions of the Celtic Margin are characterized by high-energy hydrodynamics, and tidal currents of up to 0.9 m s^{-1} have been recorded to the southeast of the Whittard Canyon (around La Chapelle Bank), although these decrease to 0.2 m s^{-1} to the northwest around the Goban Spur (Stewart *et al*., 2014). These large tidal currents are associated with equally large internal tides, guided through the major limbs of the canyon by the seafloor topography (Aslam *et al*., 2017). Near-bottom current velocities are intensified along the canyon floor, highlighting the influence of canyon topography, and can lead to high concentrations of suspended particles (Aslam *et al*., 2017; Hall *et al*., 2017). Along the Celtic Margin, the strengthening of bottom current velocities affects sediment erosion at depths of 400 – 500 m (Cunningham *et al*., 2005). The hydrodynamics across the wider region are known to transport sediments from the near shore, across the shelf and down the margin slope

(Stewart *et al*., 2014). Towards the head of the Whittard Canyon, a series of large (up to 55 m high and 200 km long) linear sand ridges were formed between 10 – 20 cal ka, orientated perpendicular to the shelf break (Scourse *et al*., 2009). These sand ridges, and sandwave fields shelfward of the canyon head, provide a source of sediment for modern transport processes. Present-day down-slope gravity flows have also been noted to transport sediment from the shelf edge down through the canyon (Amaro *et al*., 2016), and contour currents are responsible for along-slope transport of sediments across the Celtic Margin (Stewart *et al*., 2014).

FIGURE 2 – HALF PAGE (SEPARATE FILE, CAPTION AT END OF MANUSCRIPT)

3. DATA AND METHODS

Rock samples and video images from the canyon walls were collected over a four-week period during Expedition JC125 as part of the CODEMAP 2015 project (COmplex Deep-sea Ecosystems: Mapping habitat heterogeneity As Proxy for biodiversity), funded by the European Research Council (Grant No. 258482), onboard the *RRS James Cook*.

Videos were collected over 17 dives, from depths of approx. 412 to 4184 mbsl, by the Natural Environment Research Council's (NERC) *Isis* ROV, a science-class system that has a maximum dive depth of 6500 mbsl (Huvenne *et al*., 2016). The *Isis* ROV uses two different navigation systems; a Sonardyne Ultra-Short Base Line system (USBL) and a Doppler Velocity Log (DVL) dead-reckoning (Huvenne *et al*., 2016). The video imagery was collected using three optically corrected High-Definition (HD) cameras which were mounted to the front of the ROV; one camera was used primarily for piloting the vehicle, another camera was operated (pan, tilt and zoom functions) by members of the science party during

dive operations, and the third camera was kept on a fixed angle and zoom level (Huvenne *et al*., 2016).

In addition to the video footage, the ROV collected seven carbonate rock samples (representative of the lithology at each particular dive depth) which were suitable for strength testing using point load test (PLT) and uniaxial compressive strength (UCS) methods (ASTM Standards D5731–5795, 2001, and D2938-95, 2002, respectively). Due to the volume and standard dimensions of material required for UCS testing, only one rock sample recovered by the ROV was suitable for this method. The samples had average dimensions of 218.7 mm x 147.6 mm x 65.9 mm, and were acquired from the base of terraces and cliffs that exhibited erosional scars (Figure 1). The highly brittle nature of the mudstones prevented the ROV from obtaining a sample of this lithology. A single sample was acquired from a bioturbated muddy terrace within the thalweg of the western branch; this sample was classified as a soil sample in engineering property terms. All tests were conducted at room temperature, following the ISRM suggested methodologies (Franklin, 1985; Fairhurst and Hudson, 1999; Ulusay and Hudson, 2007) and ASTM standards (ASTM Standards: D4318-10, 2000; D5731–5795, 2001; D2938-95, 2002; D3148-02, 2002; D4543-04, 2004) taking into account the limited material available. The carbonate rock specimens were tested both oven dried and wet using distilled water.

FIGURE 3 – FULL PAGE (SEPARATE FILE, CAPTION AT END OF MANUSCRIPT)

4. RESULTS

4.1 BEDROCK SLOPE PROCESSES

Evidence of active erosion was observed at various depths and across a variety of different bedrock lithologies. The most prevalent of these processes was the widespread

exfoliation or spalling failure of vertical to subvertical cliff and terraced surfaces (Figure 3a & b). The most significant erosion was noted in areas of apparently weak mudstone, although occurrences of exfoliation were also noted on carbonate and chalk surfaces (Figure 3c). Typically, flakes or cobbles of mudstone were noted to have produced significant accumulations in the form of talus deposits at the base of terraces and cliffs. The exposed face above these talus slopes exhibits patches of fresh, light grey, scar surfaces often adjacent to brown, weathered surfaces unaffected by recent spalling (Figure 3b). The detritus forming the talus slopes is predominantly angular in shape, and composed of generally cobble to occasionally boulder sized clasts, with the surfaces of these slopes being notably devoid of any established benthic communities (Figure 3d). On the carbonate (predominantly chalk) units, shallow exfoliation of the exposed surface was visible in the form of flaked patches of fresh, bright white scars (devoid of benthic fauna) adjoining areas of beige, weathered surfaces that were often colonized by sessile fauna (Figure 3c).

Active retreat of terraced mudstone slopes through spalling erosion was noted on 11 separate occasions over the course of the 17 ROV dives (Figure 3a & b). Additionally, the undermining of basal sections of mudstone terraces through localized spalling failure and bioerosion was observed (Figure 3b).

In addition to spalling failure, evidence of block failure was observed in mudstone and carbonate units. In all lithologies, discontinuity orientation (bedding and joint sets) was noted to be a controlling factor, creating planes of weakness within the rock mass resulting in repeated rock slope failure. Cubic blocks of mudstone, measuring up to approx. 1.0 m in length, occur on talus slopes beneath cliffs exhibiting fresh block failure scars. These blocks occasionally displayed multiple internal fractures along parallel planes; the orientation of these fractures mirrors the failure planes that bound the toppled blocks, suggesting consistent structural weaknesses exist within the bedrock terrace above (Figure 3e). In carbonate units,

perpendicular vertical to subvertical joint sets (orientations estimated using the ROV navigation data), result in small (approx. 0.2-0.5 m) wedge block failures where bedding planes dipped out of the face of the rockwall (Figure 3f). Failure along these exposed laterally continuous bedrock ledges resulted in a "saw-tooth" profile and associated ≤0.5 m diameter diamond-shaped detachment blocks around the base of the ledge.

The mode of failure appears to be predominantly lithologically controlled, as spalling and block failures were noted at various water depths (i.e. differing pressure and temperature gradients) and in areas of varying hydrodynamic conditions (e.g. current velocities). Examples of canyon wall erosion within mudstone units were chiefly noted at water depths of between 850 – 1050 mbsl, with block failures of carbonate ledges noted at approx. 750 mbsl and spalling/exfoliation of chalk cliff faces noted between approx. 2,000 – 3,500 mbsl. It is likely that these failure mechanisms mainly reflect the physical properties of the stratigraphic units exposed in the canyon rock wall at these depths, and external factors (e.g. water temperature) play a reduced role in rock slope erosion.

Although large-scale rock slope failures (RSF) were not the main focus of this study, boulder fields were observed, particularly towards the thalweg of the canyon. These typically consisted of subrounded to subangular boulders (often >1.0 m in axial length) of mixed lithologies, embedded within the canyon floor sediments suggesting sufficient time has passed for this buildup of sediments to occur post-failure (Figure 4a & b). As many of these large clasts were in contact with adjacent boulders (as opposed to overlying), and embedded to similar depths within canyon floor sediments, this would suggest that the failure of each block occurred simultaneously or within a short timeframe. However, as no rock avalanche scars were observed in the canyon walls above, it is not possible to conclusively state whether these boulders were deposited during one catastrophic failure event or are the result of continued (and possibly ongoing) individual toppling failure episodes.

FIGURE 4 – HALF PAGE (SEPARATE FILE, CAPTION AT END OF MANUSCRIPT)

4.2 LABORATORY TEST RESULTS

The carbonate rock samples could be roughly divided into two groups based on appearance; fine to medium grained, white to yellowish grey on weathered surfaces, with open, smooth, irregular voids and no evidence of secondary carbonate precipitation. These samples were possibly oolitic and also fragmentary on weathered surfaces. Carbonate samples from the second group were fine to medium grained, very light grey to dark yellowish orange on weathered surfaces, massive with no obvious void spaces and no internal structure, and fragmentary on weathered surfaces. Samples from this group were noted to be muddier than those of the white carbonate group, in both appearance and texture. The unconsolidated sediment sample (soil in engineering terms) was identified as a silty clay through particle size analysis (Figure 5a).

The strength experiments revealed two distinct groups of carbonate rock: the muddy carbonates group which has a lower porosity and a higher strength than the pure carbonates group by a factor of about three and two to eight, respectively (Table 1 and Figure 5b). The muddy carbonates are classified as high to very high strength rocks while the pure carbonates are low to medium strength (Figure 5c) (Broch & Franklin, 1972). No clear effect on the mechanical strength could be related to the saturation condition (Figure 5b).

The plasticity plot (Figure 5d) shows the unconsolidated silty clay to be highly plastic.

TABLE 1 – FULL PAGE (FOOT OF MANUSCRIPT WITH CAPTION)

FIGURE 5 – HALF PAGE (SEPARATE FILE, CAPTION AT END OF MANUSCRIPT)

4.3 INFLUENCE OF BENTHOS ON CANYON SLOPE STABILITY

Prominent features of the surveyed mudstone terraces included shallow borings (up to approx. 2 cm diameter) and approx. 5-10 cm diameter burrows caused by benthic organisms, often clustered into highly concentrated areas (Figure 4c & d).

Spalling and exfoliation is prevalent where terrace surfaces have been extensively bored and it was noted that fresh surfaces exposed following spalling failure were devoid of borings whereas adjacent, weathered surfaces were heavily bioeroded (Figure 4c).

In addition to the shallow borings, rows of adjacent burrows were noted along the base of mudstone cliffs and terraces (up to 10 cm in diameter). These often appeared to penetrate into the strata to depths exceeding 10 cm, although it was not possible to ascertain maximum penetration depths within the terrace. Burrows were often situated within 20-50 cm of each other, resulting in sections of the base of terraces being gradually undermined.

Bioindicators of mass wasting were present across the canyon walls. These included sections of carbonate ledges and walls where the absence of coral and other sessile fauna may potentially highlight relatively recent spalling and block failures. Similar indicators were visible on slopes completely dominated by coral communities, where failure of poorly consolidated mudstone resulted in visible scars devoid of any benthic colonies.

5. DISCUSSION

Observations and data gathered during the CODEMAP 2015 research cruise to the Whittard Canyon clearly illustrate the influence that both lithology and biological activity may have upon rates of bedrock erosion over relatively short timescales.

5.1 LITHOLOGICAL CONTROLS ON ROCK SLOPE EROSION

Multiple instances of spalling failure were noted, which appeared to have the greatest influence on cliffs and terraces composed of mudstone units. This differs from other geographical locations where spalling failure has been documented in similar marine environments; for instance, this process has been observed in submarine canyons along the U.S. Atlantic Continental Margin by Chaytor *et al* (2016), where it mainly affected carbonate-rich and chalk lithologies, and not mudstone terraces as is the case in the Whittard Canyon. Observations also suggest that spalling failure and erosion of mudstone terraces may influence the stability of overlying stratigraphic units. Where active mudstone terrace retreat is occurring beneath more competent bedrock units (e.g. carbonates), and where undermining along the base of terraced slopes is taking place, there is often an increase in internal stresses within the overlying formation; this is known to result in rockfalls and toppling failures onshore (Highland and Bobrowsky, 2008), and is likely to also be true for the cases observed within the Whittard Canyon.

Block failures are controlled by inherent structural weaknesses within the bedrock units, clearly visible in the form of perpendicular joint sets. Blocks of both mud and carbonate lithologies were observed at the base of bedrock terraces where bedding planes were noted to dip out of the cliff face. These blocks exhibited similar geometries (size and orientation of surfaces), suggesting that regularly spaced joint sets are a common feature of the stratigraphic units forming the bedrock terraces.

Onshore, rock strength is known to be critical for the stability of rock slopes with outward dipping bedding planes, as the roughness of the joint provides frictional resistance against failure (Selby, 1982). As the geotechnical results revealed that the pure carbonate units were of weak to medium strength, the shearing of asperities along these joints due to slope loading or increased stresses associated with bioerosion may result in the loss of

frictional resistance and subsequently block failure. Rock slope failures from steep carbonate cliffs are not unknown; Paull *et al* (1990a) reported on fresh rock surfaces across the Florida Escarpment which they linked with episodic collapse of the limestone terraces, highlighting that subaqueous carbonate cliffs are still subjected to active erosion and modification at this present time.

In carbonate lithologies, dissolution along joints, caused by the expulsion of formation fluids, has been linked with initiating block failure by reducing the frictional resistance along discontinuities in submerged rock slopes (McHugh *et al*., 1993). Chemical weathering of joints through spring sapping has even been proposed as a model for canyon formation (e.g. Robb, 1984; Paull *et al*., 1990b), illustrating the erosive potential of fluid expulsion and migration along major joints and faults. This form of biochemical weathering is challenging to identify at individual discontinuity resolution using ROV footage, however aperture widths of >1 cm were noted within carbonate outcrops and karstic features that are typically indicative of dissolution and fluid flow were observed in chalk units.

In addition, the geotechnical testing results show that the strength of the carbonate units varies considerably depending on the apparent fine particle content; as the mud content appears to increase (based on visual descriptions of the samples), pore spaces are reduced and the carbonate unit becomes stronger. Shallow exfoliation and spalling of carbonate units may be more prevalent across these weaker, purer carbonate lithologies where the internal shear strength can be exceeded by external forces such as loading and drag from attached sessile fauna. Block failure scars were numerous in areas of visibly porous, weak carbonate ledges that were often densely populated by large communities of the clam *Acesta excavata* and associated cold-water corals, adding additional stress through gravitational and drag forcing which acts upon the intrinsically weak lithology.

It is difficult to determine why spalling and exfoliation erosion is so prevalent across the lithological units of the Whittard Canyon. The McHugh *et al* (1993) study into the role of diagenesis in exfoliation of carbonate units within submarine canyons of the U.S. Atlantic Continental Margin links the fracturing of bedrock with the volume reduction of silica-rich chalks, driven by fluid expulsion during progressive burial. As overburden is removed during canyon incision and mass wasting processes, the diagenetically formed fractures expand and exfoliation can occur (McHugh *et al*., 1993). As failure is induced by loss of support, stress release continues and erosion in the form of spalling and block failures can occur on the exposed, fractured rock surface (McHugh *et al*., 1993). In this way, a continual cycle of terrace and cliff face erosion is maintained, and provides a plausible model for the exfoliation of carbonate units within the Whittard Canyon.

Due to the highly plastic nature (atterberg limits of samples JC125_060_#1; Figure 1) and the high clay content of the sampled soil, shrink-swell behavior was considered as a factor for spalling of mudstone surfaces within the study area. However, the marine environment under which these sediments were deposited and incised should prevent such phenomenon as the clay should not shrink/swell due to it being in a fully saturated state. The potential for shrink-swell to occur would remain if these clays are bearing some non-saline water and this is exchanged for salt water. However, even if this were to occur, the effect on the volume would likely remain very small. For these reasons, shrink-swell has been discounted as being a major controlling factor on the observed spalling failure of mudstone terraces/cliffs.

The single clay sample (JC125_060_#1) represents an unconsolidated sediment terrace as opposed to a bedrock terrace, and therefore it does not give an accurate representation of the weak mudstone terraces observed elsewhere in the canyon. It is pertinent that the ROV failed to acquire a consolidated mudstone sample from the observed

bedrock terraces, due to the brittle nature of the available material, as this indicates the general weak state of the mudstone units surveyed.

5.2 EXTERNAL INFLUENCES ON BEDROCK EROSION

Other factors that may influence bedrock slope erosion include the local hydrodynamics, whereby current velocities exert increased shear stresses upon the base and surfaces of vertical walls, promoting undercutting processes and shallow quarrying of the exposed outcrops (Mitchell *et al*., 2013; Mitchell, 2014). However, as the studies by Mitchell *et al* (2013) and Mitchell (2014) highlight, bed shear stresses typically need to exceed 100 Pa before quarrying and plucking of jointed bedrock can occur and would therefore be unlikely to take place in the Whittard Canyon if relying exclusively on mean current velocities alone. Mitchell (2006; 2014) did observe that sediment flows may well produce the bed shear stresses required to initiate plucking and quarrying of bedrock within a canyon system, and turbidity currents are known to occur within the Whittard Canyon system (e.g. Cunningham *et al*., 2005).

Burrowing and boring faunal communities also play an active role in spalling failure within the Whittard canyon; it is likely that clusters of multiple borings are responsible for creating a plane of weakness subparallel to the exposed surface, controlled by the depth at which the organisms have excavated. This would result in a reduction in the rock mass strength, leading to failure (Hecker, 1982). Chaytor *et al* (2016) noted the same phenomenon in carbonate-rich lithologies within canyons along the U.S. Atlantic Continental Margin where the failure depth of surface material appeared to be controlled by the depth of bioerosion. Burrows and borings of a similar nature have been reported in exposed mudstone units in the Monterey Canyon, California, leading to bioerosion of the bedrock slope (Paull *et al.*, 2005). Burrows along the base of mudstone terraces, similar to those identified by Dillon

and Zimmerman (1970), also effectively undermine the material above, leading to a decrease in the internal strength within the rock mass, which in turn would exacerbate terrace collapse.

Analysis of the video footage suggests that sessile fauna may also influence bedrock erosion within the Whittard Canyon. In areas of block failures and shallow exfoliation surfaces associated with the carbonate units, additional loading may be applied to the terrace/cliff face through the erosive actions of sessile organisms. This can lead to an increase in drag and gravitational forces (Hecker, 1982), and could be especially pertinent within areas of the significantly weaker, pure carbonates. Sample L1, which produced very low to medium strength point load results (Is_{50} 0.051 – 0.460), was noted to be heavily encrusted with coral and other sessile organisms upon recovery from the base of the rock slope.

The bedrock erosion mechanisms observed during expedition JC125 have implications that extend beyond the area of the Whittard Canyon. While it is widely documented that slope processes around the Celtic Margin include active erosion of margin slopes, to-date studies have had a singular focus on unconsolidated sediment processes (e.g. Cunningham *et al*., 2005; Leynaud *et al*., 2009). Evidence of spalling and block failure across multiple exposed lithologies demonstrates ongoing erosion of the stratigraphic bedrock framework upon which the NE Atlantic Continental Margin sediments are draped. Given that the vast majority of the strata recovered in boreholes around the shelf and slope (e.g. Figure 2) are of carbonate or mud/clay composition, a significant proportion of the exposed bedrock terraces/cliffs along the Celtic Margin is likely to be susceptible to the aforementioned mechanisms of failure. This would suggest that the exposed bedrock cliffs and terraces are in fact active and not inert features of the margin slopes.

Chaytor *et al* (2016) used the presence (and absence) of slow growing corals and sponges to demonstrate long-term stability of canyon rockwalls and relative timings of rock

slope failures across canyons of the U.S. Atlantic Continental Margin. While no baseline data is available to ascertain rates of erosion, the observed failure surfaces exhibited clear fresh, and therefore relatively recent, scars and slopes were often devoid of benthic communities implying recolonization had probably not taken place yet. Many erosional scars, which were fresh in appearance with no benthic faunal communities attached, were surrounded by well-established coral communities suggesting relatively recent failure of the slope surface. In relation to the wider Celtic Margin and Whittard Canyon system, the large-scale sediment slumps that have been documented are singular events that are likely to be relatively infrequent when compared with the bedrock erosional processes.

The spalling of bedrock terraces and structurally-controlled block failures, coupled with the geotechnical laboratory results, suggest that morphological alteration of the rockwalls that underpin the Whittard Canyon is currently ongoing. In addition, morphological modification of rock slopes through bioerosion was noted across several ROV dives. A limited number of studies have noted these erosional processes in submarine canyons across both active and passive margins elsewhere; Chaytor *et al* (2016) highlighted the presence of similar spalling failures associated with clusters of borings in carbonate units forming submarine canyon rockwalls across the U.S. Atlantic Continental Margin, and Paull *et al* (2005) reported on notches, small caves and burrows penetrating and modifying mudstone slopes that had become exposed through the mass wasting of overlying sediments within the Monterey Canyon, California. This would suggest that these processes have wide implications for the stability of submarine canyon rockwalls on a global scale. Furthermore, research undertaken by Paull *et al* (1990a) on the Florida Escarpment also highlights that these erosional processes influence the morphology of subaqueous bedrock slopes in different geological settings and are therefore not only limited to rockwalls within submarine canyons.

Further work to better define the contribution of these small-scale processes on canyon evolution, which have been underestimated until the present day is still required, especially in relation to the physical properties of bedrock units. In addition, further studies on the influence of benthic fauna on the modification of rock slope morphology within submarine canyons would be beneficial. At present, the role that rock slope erosion has upon sediment transfer and quantitative budgets within submarine canyons has not been determined, and this should also be investigated further.

6. CONCLUSIONS

ROV observations coupled with geotechnical laboratory measurements have allowed for a detailed assessment of the Whittard Canyon rockwalls to be undertaken. The following conclusions can be drawn; (1) Ongoing spalling erosion is prevalent throughout the canyon, particularly affecting brittle mudstone units. This process results in the build-up of substantial talus slopes at the base of eroding terraces, and may lead to the undermining of more competent units above; (2) Block failures within carbonate units are controlled by the orientation of discontinuity joint sets, in addition to intrinsic strength properties which appear to be influenced by the fine mud content (and therefore the available pore space) of the lithology and; (3) Benthic organisms have the potential to exacerbate slope erosion in several ways, and evidence of ongoing bioerosion was observed across mudstone and carbonate lithologies.

Due to a lack of published data relating to submarine canyon rockwalls, it is impossible to confirm that these erosional processes also occur at similar rates and with similar results in submarine canyons worldwide. However, some of the processes described above have been noted in canyons along the U.S. NW Atlantic Margin (Chaytor *et al*., 2016) and within the Monterey Canyon, California (Paull *et al*., 2005). Our results highlight the

requirement for further studies to assess the contribution of the observed processes in canyon evolutionary models and to better understand the interactive processes between benthic communities and mass failure within submarine canyons.

ACKNOWLEDGEMENTS

This work was made possible by the CODEMAP 2015 research expedition to the Whittard Canyon, Celtic Margin (funded by ERC Starting Grant 258482 and the NERC MAREMAP programme). A special thank you to all members of the CODEMAP 2015 science team, and the captain and crew of the *RRS James Cook*. Gareth Carter publishes with permission of the Director of the British Geological Survey (Natural Environment Research Council). The authors would like to extend their sincerest gratitude to the reviewers (Katherine Maier, United States Geological Survey, and Neil Mitchell, University of Manchester, UK) and the Guest Editor (Pere Puig, Spanish National Research Council) for their hugely constructive and encouraging feedback and comments on this manuscript. The authors are also grateful to Emrys Phillips, British Geological Survey, for internal review of the manuscript before submission.

REFERENCES

Amaro, T., Huvenne, V. A. I., Allcock, A. L., Aslam, T., Davies, J. S., Danovaro, R., De Stigter, H. C., Duineveld, G. C. A., Gambi, C., Gooday, A. J., Gunton, L. M., Hall, R., Howell, K. L., Ingels, J., Kiriakoulakis, K., Kershaw, C. E., Lavaleye, M. S. S., Robert, K., Stewart, H., Van Rooij, D., White, M. and Wilson, A.M. (2016). The Whittard Canyon – A case study of submarine canyon processes. *Progress in Oceanography, 146*, 38–57.

Aslam, T., Hall, R. A., & Dye, S. R. (2017). Internal tides in a dendritic submarine canyon. *Progress in Oceanography*.

ASTM Standard D2938-95, 2002, Standard Test Method for Unconfined Compressive Strength of Intact Rock Core Specimens: ASTM International, West Conshohocken, PA, www.astm.org.

ASTM Standard D3148-02, 2002, Standard Test Method for Elastic Moduli of Intact Rock Core Specimens in Uniaxial Compression: ASTM International, West Conshohocken, PA, www.astm.org.

ASTM Standard D4318-10, 2000, Standard test methods for liquid limit, plastic limit, and plasticity index of soils: ASTM International, West Conshohocken, PA, www.astm.org.

ASTM Standard D4543-04, 2004, Standard Practices for Preparing Rock Core Specimens and Determining Dimensional and Shape Tolerances: ASTM International, West Conshohocken, PA, www.astm.org.

ASTM Standard D5731–5795, 2001, Standard method for determination of the point load strength index of rock: ASTM International, West Conshohocken, PA, www.astm.org.

Broch, E. and Franklin, J. A. (1972). The point-load strength test. *International Journal of Rock Mechanics and Mining Sciences & Geomechanics Abstracts, 9*, 669–676.

Chaytor, J. D., Demopoulos, A. W. J., ten Brink, U. S., Baxter, C., Quattrini, A. M. and Brothers, D. S. (2016). Assessment of Canyon Wall Failure Process from Multibeam Bathymetry and Remotely Operated Vehicle (ROV) Observations, U.S. Atlantic Continental Margin. In G. Lamarche, J. Mountjoy, S. Bull, T. Hubble, S. Krastel, E. Lane, A. Micallef, L. Moscardelli, C. Mueller, I. Pecher, and S. Woelz (Eds.), *Submarine Mass Movements and their Consequences, 7th International Symposium* (pp. 103–113). Switzerland, Springer International Publishing.

Cunningham, M. J., Hodgson, S., Masson, D. G. and Parson, L. M. (2005). An evaluation of along-and down-slope sediment transport processes between Goban Spur and Brenot Spur on the Celtic Margin of the Bay of Biscay. *Sedimentary Geology, 79*(1), 99–116.

Dillon, W. P. and Zimmerman, H. B. (1970). Erosion by biological activity in two New England submarine canyons. *Journal of Sedimentary Research, 40*(2), 542-547.

Evans, C. D. R. and Hughes, M. J. (1984). The Neogene succession of the South Western Approaches, Great Britain. *Journal of the Geological Society, 141*(2), 315–326.

Evans, C. D. R. (1990) *The geology of the western English Channel and its western approaches*. London, HMSO for the British Geological Survey, 93 p.

Fairhurst, C. E. and Hudson, J. A. (1999). Draft ISRM suggested method for the complete stress-strain curve for intact rock in uniaxial compression, ISRM suggested methods (SMs): second series. *International Journal of Rock Mechanics and Mining Sciences, 36*, 279–289.

Franklin, J. A. (1985). Suggested method for determining point load strength, ISRM suggested methods. *International Journal of Rock Mechanics and Mining Sciences & Geomechanics Abstracts, 22*, 51–60.

Hall, R. A., Aslam, T., & Huvenne, V. A. (2017). Partly standing internal tides in a dendritic submarine canyon observed by an ocean glider. *Deep Sea Research Part I: Oceanographic Research Papers*.

Hecker, B. (1982). Possible benthic fauna and slope instability relationships. In S. Saxov and J. K. Nieuwenhuis (Eds.), *Marine Slides and Other Mass Movements* (pp. 335–347). New York, Plenum.

Highland, L. and Bobrowsky, P. T. (2008). The landslide handbook: a guide to understanding landslides (p. 129). Reston, U.S. Geological Survey.

Huvenne, V. A. I., Wynn, R. B. and Gales, J. A. (2016). RRS James Cook Cruise 124-125-126. CODEMAP2015: Habitat mapping and ROV vibrocorer trials around Whittard Canyon and Haig Fras. National Oceanography Centre Open-File Report (Cruise Report No. 36).

Leynaud, D., Mienert, J. and Vanneste, M. (2009). Submarine mass movements on glaciated and non-glaciated European continental margins: a review of triggering mechanisms and preconditions to failure. *Marine and Petroleum Geology, 26*(5), p. 618–632.

Lo Iacono, C., Sulli, A., Agate, M., Lo Presti, V., Pepe, F. and Catalano, R. (2011). Submarine canyon morphologies in the Gulf of Palermo (Southern Tyrrhenian Sea) and possible implications for geo-hazard. *Marine Geophysical Research, 32*(1-2), 127–138, doi:10.1007/s11001-011-9118-0.

McHugh, C. M., Ryan, W. B. and Schreiber, B. C. (1993). The role of diagenesis in exfoliation of submarine canyons. *AAPG Bulletin, 77*(2), 145-172.

Micallef, A., Mountjoy, J. J., Canals, M. and Lastras, G. (2012). Deep-seated bedrock landslides and submarine canyon evolution in an active tectonic margin: Cook Strait, New Zealand. In Y. Yamada, K. Kawamura, K. Ikehara, Y. Ogawa, R. Urgeles, D. Mosher, J. Chaytor, and M. Strasser (Eds.), *Submarine Mass Movements and their Consequences, 5th International Symposium* (pp. 201–212). Netherlands, Springer.

Mitchell, N. C. (2006). Morphologies of knickpoints in submarine canyons. *Geological Society of America Bulletin, 118*(5-6), 589-605.

Mitchell, N. C., Huthnance, J. M., Schmitt, T. and Todd, B. (2013). Threshold of erosion of submarine bedrock landscapes by tidal currents. *Earth Surface Processes and Landforms, 38*(6), 627-639.

Mitchell, N. C. (2014). Bedrock erosion by sedimentary flows in submarine canyons. *Geosphere, 10*(5), 892-904.

Montadert, L., Roberts, D. G., Auffret, G. A., Bock, W. D., Dupeuble, P. A., Hailwood, E. A., Harrison, W. E., Kagami, H., Lumsden, D. N., Muller, C. M., Schnitker, D., Thompson, R. W., Thompson, T. L., Timofeev, P. P., and Mann, D. (1979). Deep Sea Drilling Project (DSDP), Site 402/Hole 402A, doi:10.2973/dsdp.proc.48.105.1979.

Paull, C. K., Freeman-Lynde, R., Bralower, T. J., Gardemal, J. M., Neumann, A. C., D'Argenio, B. and Marsella, E. (1990a). Geology of the strata exposed on the Florida Escarpment. *Marine Geology, 91*(3), 177-194.

Paull, C. K., Spiess, F. N., Curray, J. R. and Twichell, D. C. (1990b). Origin of Florida Canyon and the role of spring sapping on the formation of submarine box canyons. *Geological Society of America Bulletin, 102*(4), 502-515.

Paull, C. K., Ussler, W., Greene, H. G., Barry, J. and Keaten, R. (2005). Bioerosion by chemosynthetic biological communities on Holocene submarine slide scars. *Geo-Marine Letters, 25*(1), 11-19.

Puig, P., Ogston, A. S., Mullenbach, B. L., Nittrouer, C. A., & Sternberg, R. W. (2003). Shelf-to-canyon sediment-transport processes on the Eel continental margin (northern California). *Marine Geology, 193*(1), 129-149.

Puig, P., Palanques, A., and Martín, J. (2014). Contemporary sediment-transport processes in submarine canyons. *Annual review of marine science, 6*, 53-77.

Robb, J. M. (1984). Spring sapping on the lower continental slope, offshore New Jersey. *Geology, 12*(5), 278-282.

Rowe, G. T. (1974). The effects of the benthic fauna on the physical properties of deep-sea sediments. In A. Inderbitzen (Ed.), *Deep-Sea Sediments: Physical and Mechanical Properties* (pp. 381–400). New York, Springer.

Scourse, J., Uehara, K., and Wainwright, A. (2009). Celtic Sea linear tidal sand ridges, the Irish Sea Ice Stream and the Fleuve Manche: palaeotidal modelling of a transitional passive margin depositional system. *Marine Geology, 259*(1), 102-111.

Selby, M. J. (1982). Controls on the stability and inclinations of hillslopes formed on hard rock. *Earth Surface Processes and Landforms, 7*(5), 449-467.

Stewart, H. A., Davies, J. S., Guinan, J. and Howell, K. L. (2014). The Dangeard and Explorer canyons, South Western Approaches UK: Geology, sedimentology and newly discovered cold-water coral mini-mounds. *Deep Sea Research Part II: Topical Studies in Oceanography, 104*, 230–244.

Sultan, N., Gaudin, M., Berne, S., Canals, M., Urgeles, R. and Lafuerza, S. (2007). Analysis of slope failures in submarine canyon heads: an example from the Gulf of Lions. *Journal of Geophysical Research: Earth Surface, 112*(F1), doi:10.1029/2005JF000408.

Sumner, E. J., Peakall, J., Dorrell, R. M., Parsons, D. R., Darby, S. E., Wynn, R. B., McPhail, S. D., Perrett, J., Webb, A., and White, D. (2014). Driven around the bend: Spatial evolution and controls on the orientation of helical bend flow in a natural submarine gravity current. *Journal of Geophysical Research: Oceans, 119*(2), 898-913.

Talling, P. J. (2014). On the triggers, resulting flow types and frequencies of subaqueous sediment density flows in different settings. *Marine Geology, 352*, 155-182.

Ulusay, R. and Hudson, J. A. (2007). The complete ISRM suggested methods for rock characterization, testing and monitoring: 1974-2006. In R. Ulusay and J. A. Hudson (Eds.), *Commission on testing methods. International Society of Rock Mechanics. Compilation arranged by ISRM Turkish National Group*. Turkey, Springer.

Valentine, P. C., Uzmann, J. R. and Cooper, R. A. (1980). Geologic and biologic observations in Oceanographer submarine canyon: descriptions of dives aboard the research submersibles Alvin (1967, 1978) and Nekton Gamma (1974). *U.S. Geological Survey Open File Report*, 80–76: 40 pp.

Warme, J. E., Slater, R. A. and Cooper, R. A. (1978). Bioerosion in submarine canyons. In D. J. Stanley and G. Kelling (Eds.), *Sedimentation in submarine canyons, fans, and trenches*. Stroudsburg, Pennsylvania, Dowden, Hutchinson and Ross, p. 65–70.

FIGURE AND TABLE CAPTIONS

Figure 1: Location of study area (red box) is inset, with locations of boreholes displayed (orange dot for BGS borehole and yellow dots for DSDP boreholes). Main figure shows hillshaded bathymetric map of the Whittard Canyon gridded to 50 m overlying GEBCO data. Locations of rock samples and bedrock erosion observations are shown.

Figure 2: (A) BGS borehole +49-009/42 (K.B. Kelly Bushing) and (B) DSDP borehole 402, illustrating regional stratigraphy across the shelf and slope into which the Whittard Canyon is incised (adapted from Montadert *et al*., 1979).

Figure 3: (a) & (b) show spalling/exfoliation surfaces on mudstone terraces, resulting in cliffline retreat; (c) exfoliation on a chalk cliff surface; (d) extensive accumulations of mudstone material at base of spalling terrace, forming a talus slope; and (e) & (f) show structurally controlled block failures in mudstone and carbonate units respectively.

Figure 4: (a) & (b) boulders of mixed lithologies embedded in canyon floor sediments; (c) shallow borings cover the terrace surface to the left of the image, whereas the fresh, exfoliation surface is devoid of borings and; (d) larger borings penetrating a weathered mudstone terrace.

Figure 5: Summary of geotechnical results (a) grain size analysis of the unconsolidated sediment sample, showing it to be a silty clay; (b) effective porosity vs strength (c) rock strength (Point Load Test & Unconfined Compressive Strength) of pure carbonates and muddy carbonates (d) plasticity plot for silty clay sample.

Table 1: Point Load Index (PLI) testing results, showing the difference in strength values between pure and muddy carbonate samples.

Sample ID	Sample Type	Depth (mbsl)	Latitude	Longitude	Is_{50}
L1a	pure carbonate	-736.30	48.759976	-10.458456	0.263
L1b	pure carbonate	-736.30	48.759976	-10.458456	0.252
L1c	pure carbonate	-736.30	48.759976	-10.458456	0.223
L1d	pure carbonate	-736.30	48.759976	-10.458456	0.280
L1e	pure carbonate	-736.30	48.759976	-10.458456	0.209
L1f	pure carbonate	-736.30	48.759976	-10.458456	0.401
L1g	pure carbonate	-736.30	48.759976	-10.458456	0.079
L1h	pure carbonate	-736.30	48.759976	-10.458456	0.120
L1i	pure carbonate	-736.30	48.759976	-10.458456	0.333
L1j	pure carbonate	-736.30	48.759976	-10.458456	0.460
L1k	pure carbonate	-736.30	48.759976	-10.458456	0.100
L1l	pure carbonate	-736.30	48.759976	-10.458456	0.088
L1m	pure carbonate	-736.30	48.759976	-10.458456	0.073
L1n	pure carbonate	-736.30	48.759976	-10.458456	0.080
L1o	pure carbonate	-736.30	48.759976	-10.458456	0.051
L1p	pure carbonate	-736.30	48.759976	-10.458456	0.135
L1q	pure carbonate	-736.30	48.759976	-10.458456	0.081
L2a	pure carbonate	-491.50	48.737467	-10.090386	0.263
L2b	pure carbonate	-491.50	48.737467	-10.090386	0.306
L2c	pure carbonate	-491.50	48.737467	-10.090386	0.212
L2d	pure carbonate	-491.50	48.737467	-10.090386	0.366
L2e	pure carbonate	-491.50	48.737467	-10.090386	0.268
L2f	pure carbonate	-491.50	48.737467	-10.090386	0.245
L2g	pure carbonate	-491.50	48.737467	-10.090386	0.282
L2h	pure carbonate	-491.50	48.737467	-10.090386	0.211
L2i	pure carbonate	-491.50	48.737467	-10.090386	0.163
L3a	pure carbonate	-874.00	48.735818	-10.099441	0.121
L3b	pure carbonate	-874.00	48.735818	-10.099441	0.338
L4a	pure carbonate	-760.30	48.760368	-10.461013	0.345
#5a	muddy carbonate	-838.00	48.753295	-10.472528	2.382
#5b	muddy carbonate	-838.00	48.753295	-10.472528	2.527
#6a	muddy carbonate	-841.00	48.753296	-10.472546	3.045
#6b	muddy carbonate	-841.00	48.753296	-10.472546	2.608
#6c	muddy carbonate	-841.00	48.753296	-10.472546	2.729
#6d	muddy carbonate	-841.00	48.753296	-10.472546	2.064
#6e	muddy carbonate	-841.00	48.753296	-10.472546	0.845
#6f	muddy carbonate	-841.00	48.753296	-10.472546	2.716
#6g	muddy carbonate	-841.00	48.753296	-10.472546	2.364
#6h	muddy carbonate	-841.00	48.753296	-10.472546	2.233
#6i	muddy carbonate	-841.00	48.753296	-10.472546	0.585

Table 2: Point Load Index (PLI) testing results, showing the difference in strength values between pure and muddy carbonate samples.

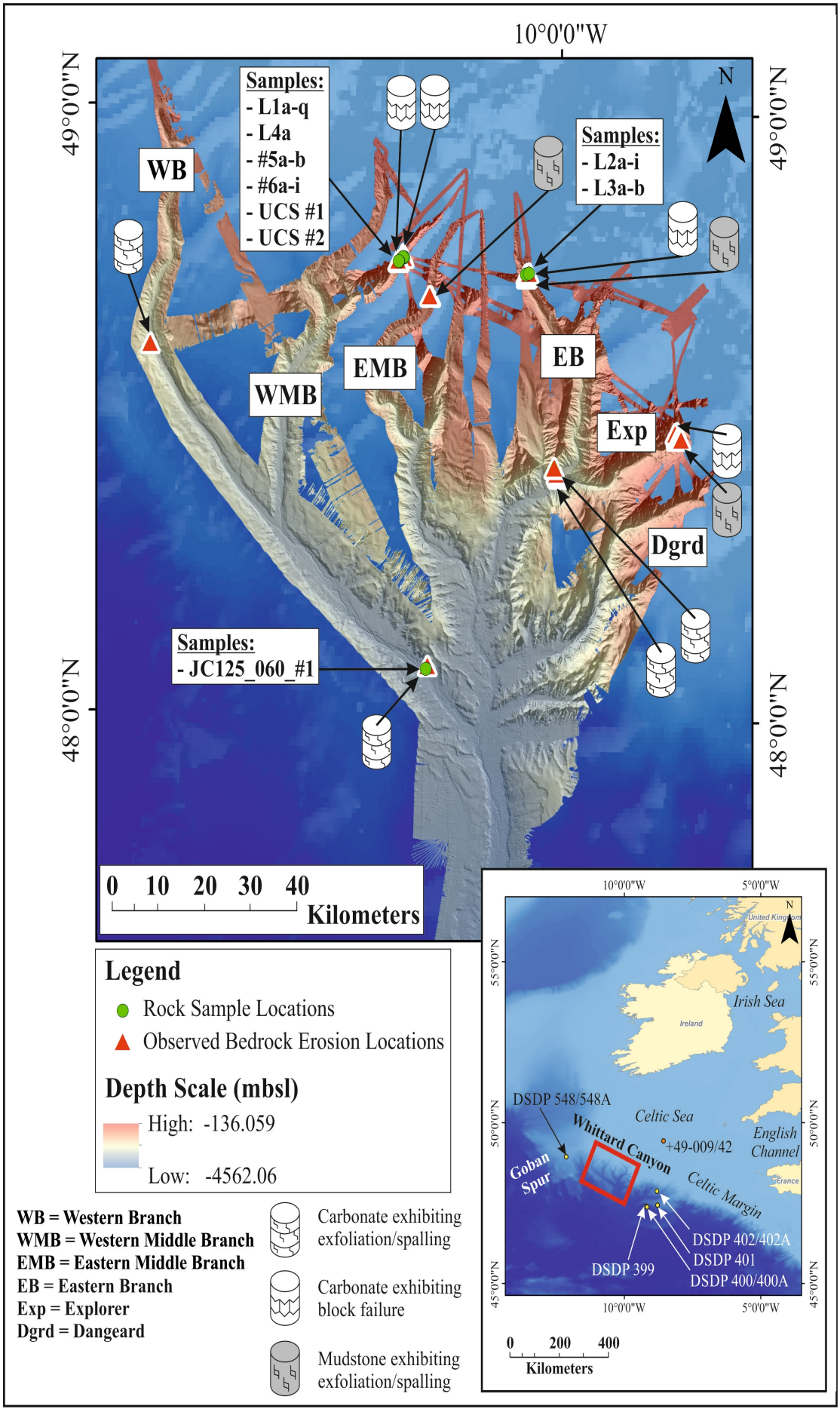
10°0'0"W
49°0'0"N
48°0'0"N
N
Samples:
- L1a-q
- L4a
- #5a-b
- #6a-i
- UCS #1
- UCS #2
Samples:
- L2a-i
- L3a-b
Samples:
- JC125_060_#1
WB
WMB
EMB
EB
Exp
Dgrd
0 10 20 30 40
Kilometers
Legend
Rock Sample Locations
Observed Bedrock Erosion Locations
Depth Scale (mbsl)
High: -136.059
Low: -4562.06
WB = Western Branch
WMB = Western Middle Branch
EMB = Eastern Middle Branch
EB = Eastern Branch
Exp = Explorer
Dgrd = Dangeard
Carbonate exhibiting exfoliation/spalling
Carbonate exhibiting block failure
Mudstone exhibiting exfoliation/spalling
10°0'0"W
5°0'0"W
55°0'0"N
50°0'0"N
45°0'0"N
Irish Sea
Ireland
Celtic Sea
English Channel
Celtic Margin
Whittard Canyon
Goban Spur
DSDP 548/548A
+49-009/42
DSDP 399
DSDP 402/402A
DSDP 401
DSDP 400/400A
0 200 400
Kilometers

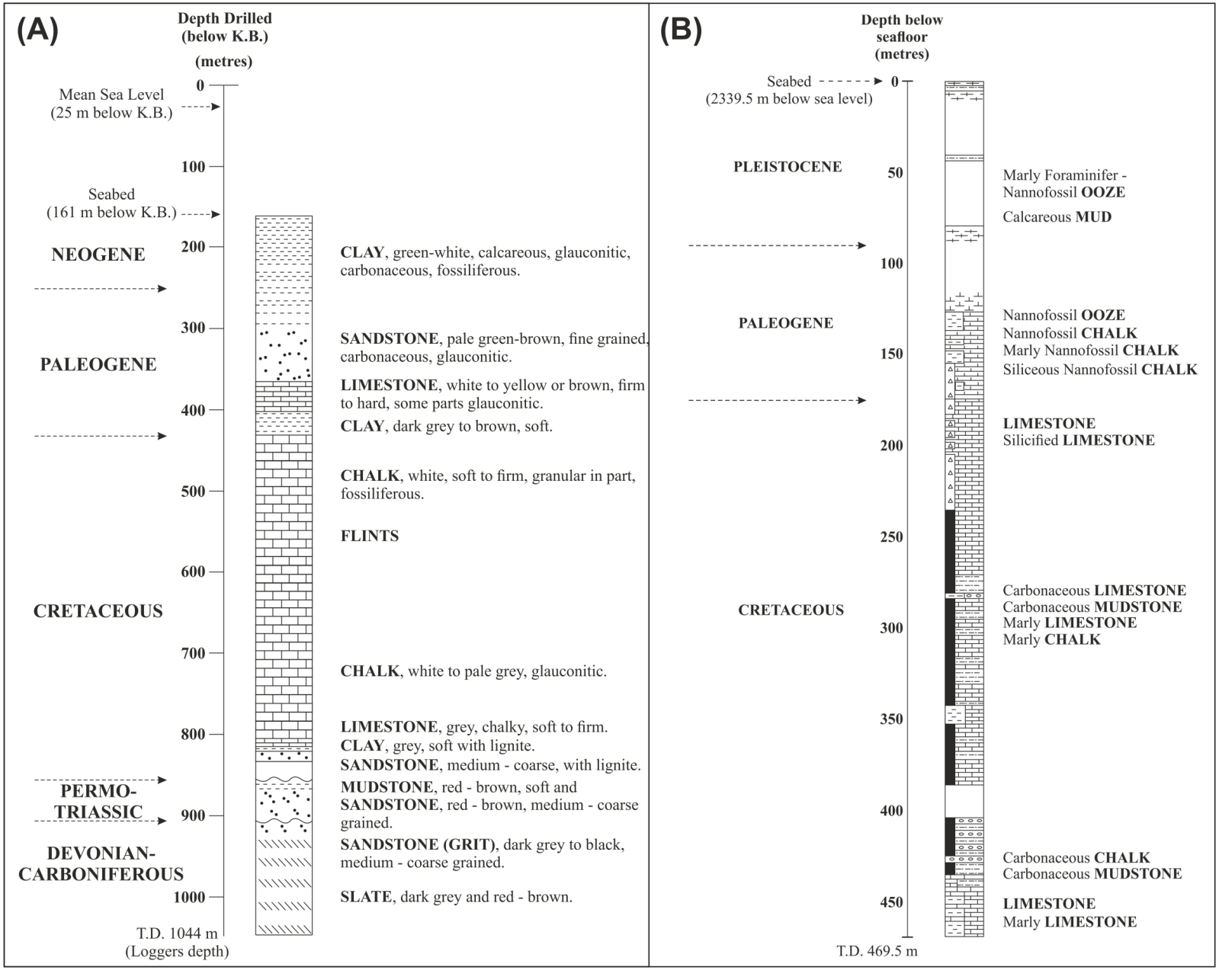
(A)
Depth Drilled
(below K.B.)
(metres)
Mean Sea Level
(25 m below K.B.)
Seabed
(161 m below K.B.)
NEOGENE
PALEOGENE
CRETACEOUS
PERMO-
TRIASSIC
DEVONIAN-
CARBONIFEROUS
0
100
200
300
400
500
600
700
800
900
1000
T.D. 1044 m
(Loggers depth)
CLAY, green-white, calcareous, glauconitic, carbonaceous, fossiliferous.
SANDSTONE, pale green-brown, fine grained, carbonaceous, glauconitic.
LIMESTONE, white to yellow or brown, firm to hard, some parts glauconitic.
CLAY, dark grey to brown, soft.
CHALK, white, soft to firm, granular in part, fossiliferous.
FLINTS
CHALK, white to pale grey, glauconitic.
LIMESTONE, grey, chalky, soft to firm.
CLAY, grey, soft with lignite.
SANDSTONE, medium - coarse, with lignite.
MUDSTONE, red - brown, soft and
SANDSTONE, red - brown, medium - coarse grained.
SANDSTONE (GRIT), dark grey to black, medium - coarse grained.
SLATE, dark grey and red - brown.
(B)
Depth below
seafloor
(metres)
Seabed
(2339.5 m below sea level)
PLEISTOCENE
PALEOGENE
CRETACEOUS
0
50
100
150
200
250
300
350
400
450
T.D. 469.5 m
Marly Foraminifer -
Nannofossil OOZE
Calcareous MUD
Nannofossil OOZE
Nannofossil CHALK
Marly Nannofossil CHALK
Siliceous Nannofossil CHALK
LIMESTONE
Silicified LIMESTONE
Carbonaceous LIMESTONE
Carbonaceous MUDSTONE
Marly LIMESTONE
Marly CHALK
Carbonaceous CHALK
Carbonaceous MUDSTONE
LIMESTONE
Marly LIMESTONE

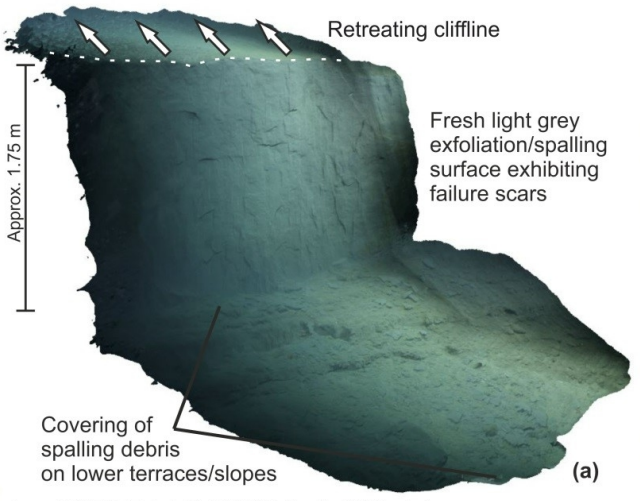

Lon: -9.6570247; Lat: 48.4756348; Depth: 852.6 mbsl

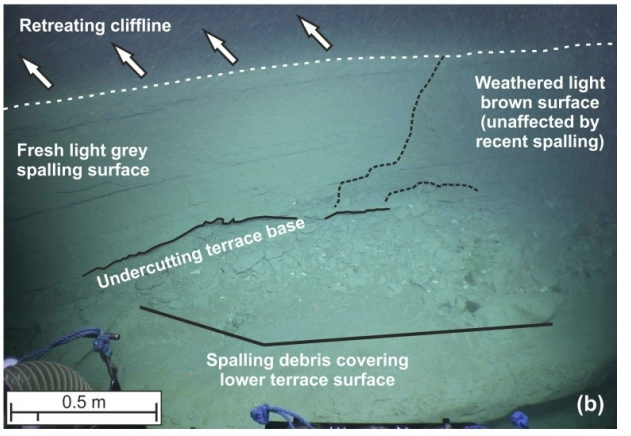

Lon: -9.6535018; Lat: 48.4675862; Depth: 1017.5 mbsl

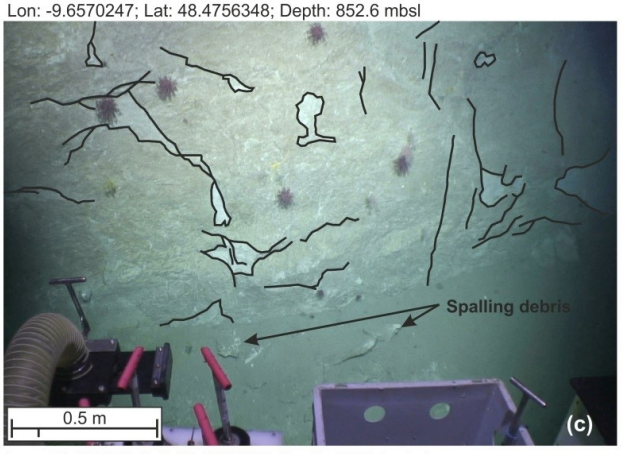

Lon: -11.199363; Lat: 48.6075657; Depth: 2617.1 mbsl

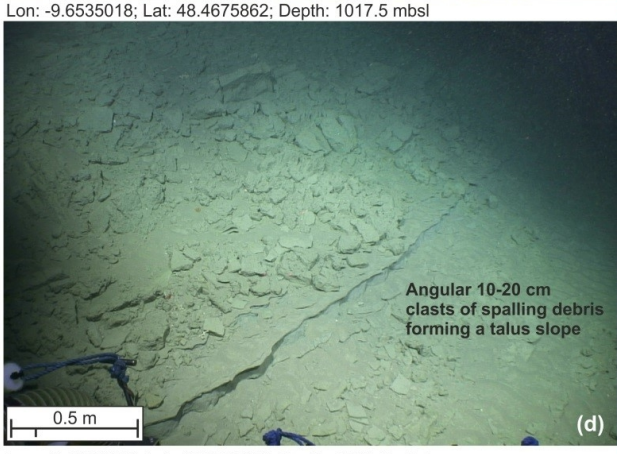

Lon: -9.6537852; Lat: 48.4693107; Depth: 1001.6 mbsl

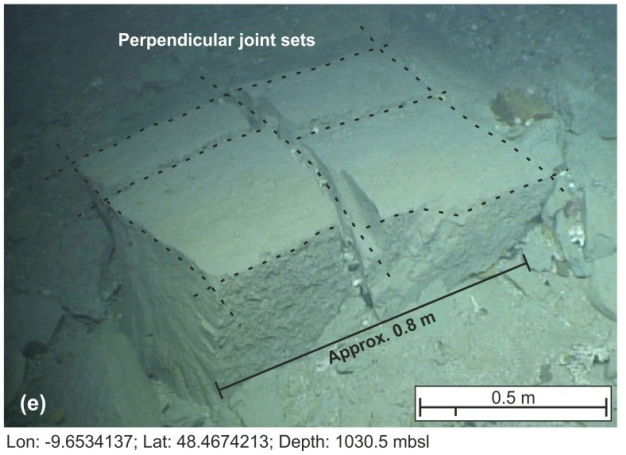

Lon: -9.6534137; Lat: 48.4674213; Depth: 1030.5 mbsl

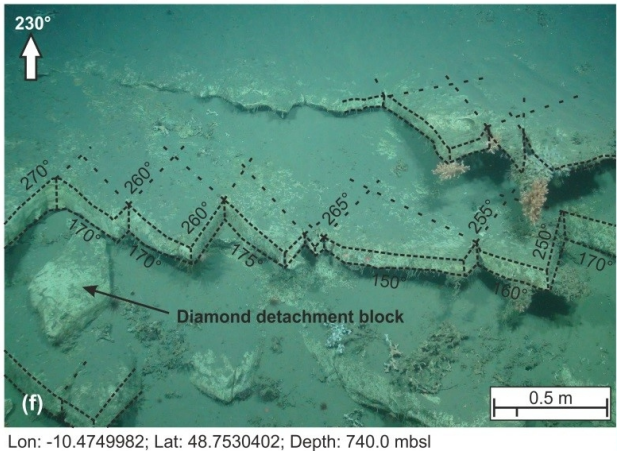

Lon: -10.4749982; Lat: 48.7530402; Depth: 740.0 mbsl

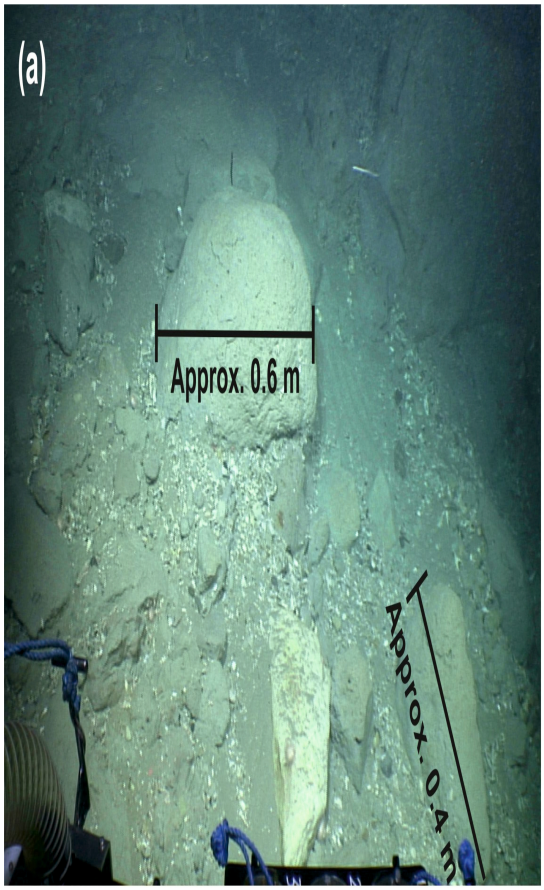

Lon: -9.6527113; Lat: 48.4660002; Depth: 1065.8 mbsl

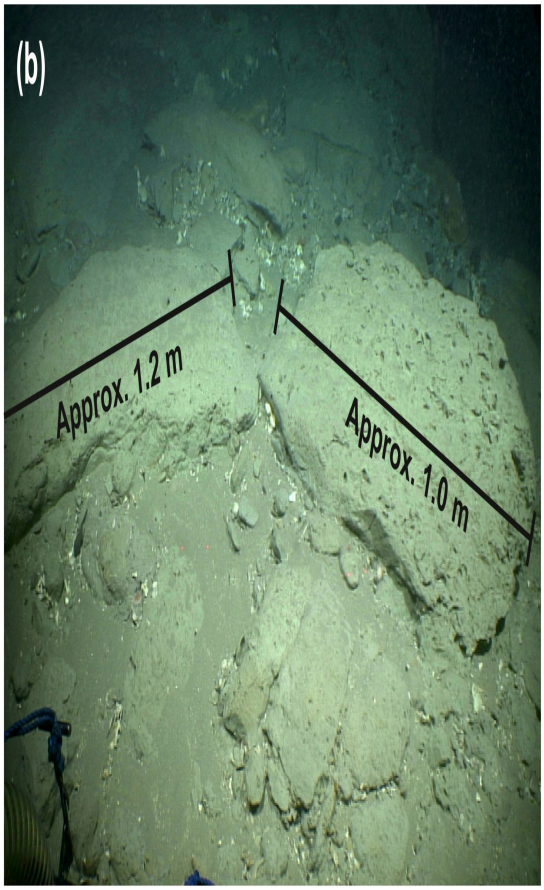

Lon: -9.6527818; Lat: 48.4660627; Depth: 1064.8 mbsl

Lon: -9.639216; Lat: 48.465525; Depth: 736.2 mbsl

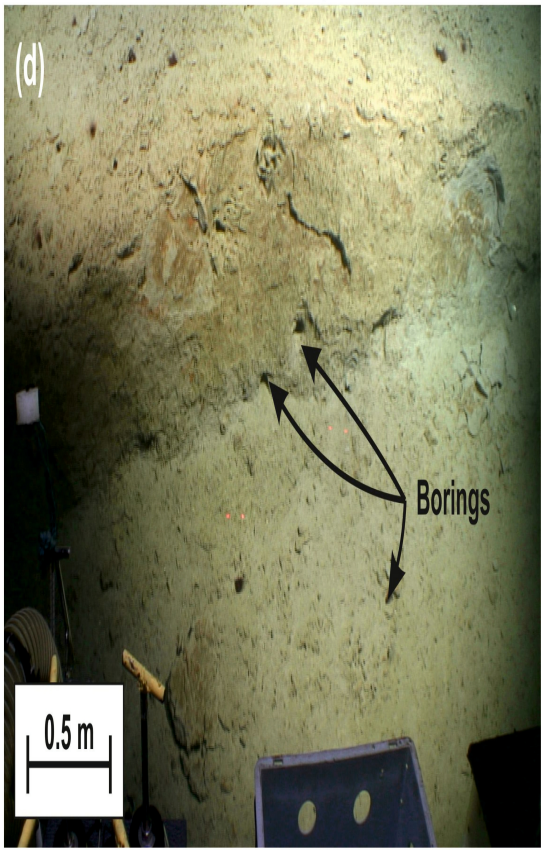

Lon: -9.6429888; Lat: 48.4673043; Depth: 864.2 mbsl

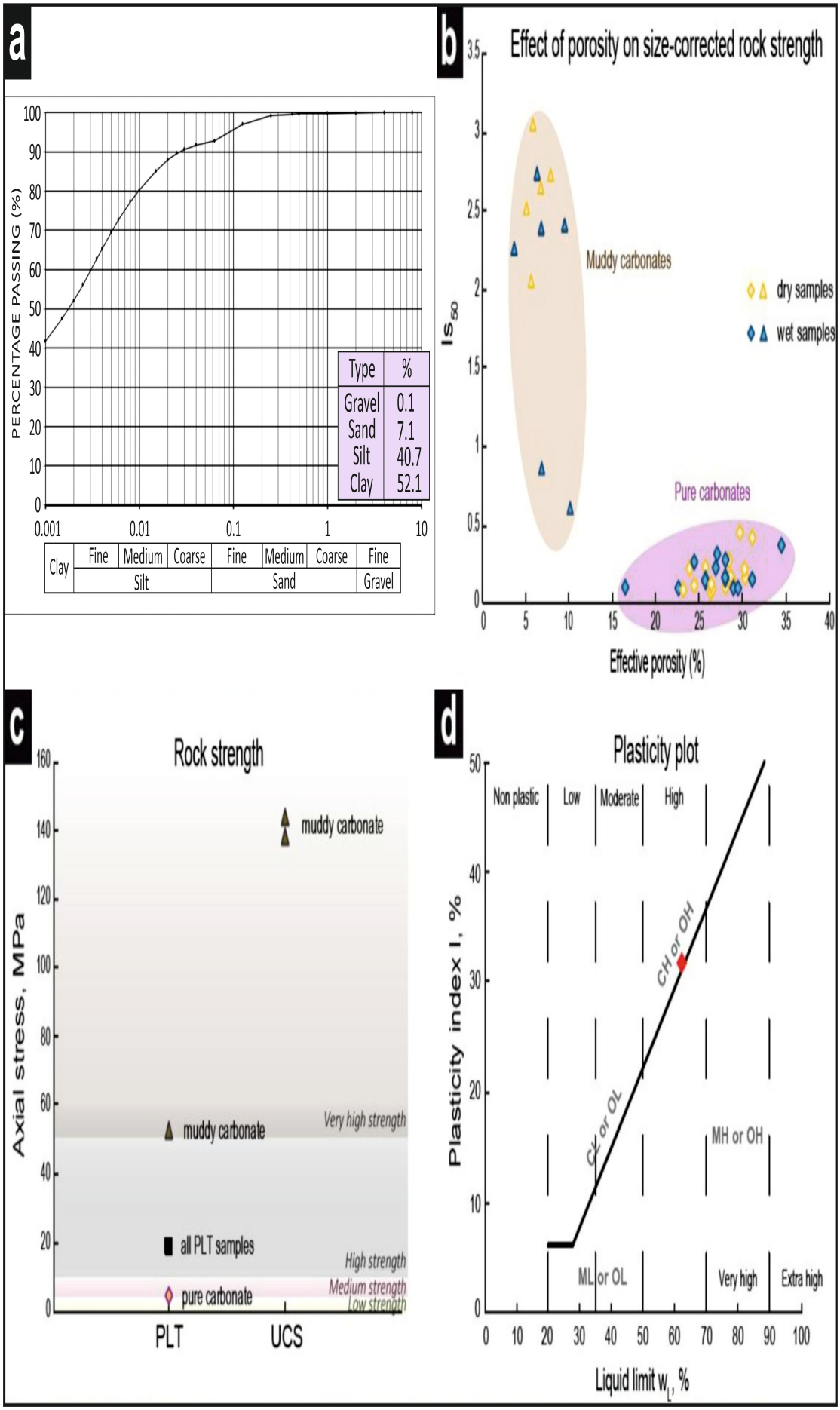
a
PERCENTAGE PASSING (%)
100
90
80
70
60
50
40
30
20
10
0
0.001
0.01
0.1
1
10
Type | %
Gravel | 0.1
Sand | 7.1
Silt | 40.7
Clay | 52.1
Clay
Fine
Medium
Coarse
Fine
Medium
Coarse
Fine
Silt
Sand
Gravel
b
Effect of porosity on size-corrected rock strength
Is50
Muddy carbonates
Pure carbonates
dry samples
wet samples
Effective porosity (%)
c
Rock strength
Axial stress, MPa
muddy carbonate
muddy carbonate
all PLT samples
pure carbonate
Very high strength
High strength
Medium strength
Low strength
PLT
UCS
d
Plasticity plot
Non plastic
Low
Moderate
High
CH or OH
CL or OL
MH or OH
ML or OL
Very high
Extra high
Plasticity index I, %
Liquid limit wL, %